Hybrid functional studies of the oxygen vacancy in TiO_2

A. Janotti,[1] J. B. Varley,[1] P. Rinke,[1] N. Umezawa,[1,*] G. Kresse,[2] and C. G. Van de Walle[1]
[1]*Materials Department, University of California, Santa Barbara, California 93106-5050, USA*
[2]*Faculty of Physics, Center for Computational Materials Science, University of Vienna, A-1090 Wien, Austria*
(Received 4 May 2009; revised manuscript received 31 December 2009; published 16 February 2010)

The electronic and structural properties of the oxygen vacancy (V_O) in rutile TiO_2 are studied using generalized Kohn-Sham theory with the Heyd, Scuseria, and Ernzerhof (HSE) hybrid functional for exchange and correlation. The HSE approach corrects the band gap and allows for a proper description of defects with energy levels close to the conduction band. According to the HSE calculations, V_O is a shallow donor for which the +2 charge state is lower in energy than the neutral and +1 charge states for all Fermi-level positions in the band gap. The formation energy of V_O^{2+} is relatively low in *n*-type TiO_2 under O-poor conditions but it rapidly increases with the oxygen chemical potential. This is consistent with experimental observations where the electrical conductivity decreases with oxygen partial pressure.

DOI: 10.1103/PhysRevB.81.085212 PACS number(s): 71.55.−i, 61.72.Bb

I. INTRODUCTION

TiO_2 is a material of increasing interest in electronics and optoelectronics, with applications in high-*k* dielectrics, solar cells, and photocatalysis.[1–5] Rutile TiO_2 has a wide band gap of 3.1 eV and exhibits a tendency for unintentional *n*-type conductivity.[6–12] Understanding and controlling this conductivity would be a key step toward the application of TiO_2 as a semiconductor. It has been widely reported that the *n*-type conductivity in TiO_2 varies inversely with the oxygen partial pressure in the annealing atmosphere.[7–12] These observations have led to the conclusion that oxygen vacancies are the cause of the *n*-type conductivity.[4,9–13] It has also been argued that TiO_2 can be easily reduced, and that it supports a high degree of nonstoichiometry in the form of oxygen vacancies (TiO_{2-x}).[4,13–15] Despite the many years of research on TiO_2, direct evidence of the role of oxygen vacancies in the *n*-type conductivity is still lacking, and a microscopic understanding of the electronic and structural properties of the oxygen vacancy has remained elusive. Most experiments have focused on the surface of rutile TiO_2, and it is not clear whether annealing under oxygen-poor or oxygen-rich atmospheres truly affects the material as a whole or only a thin surface layer. Unintentional incorporation of dopant impurities, such as hydrogen, may further complicate the interpretation of electrical measurements. In addition, for ZnO both experiment and theory have recently shown that, contrary to conventional wisdom, the oxygen vacancy is a deep rather than a shallow donor.[16–18] It is therefore opportune to revisit the role of oxygen vacancy V_O in bulk TiO_2.

Density-functional theory (DFT) has become the method of choice for studying the electronic structure of isolated point defects in semiconductors and insulators.[19] The most common exchange-correlation functionals in this context are the local-density approximation (LDA) or the generalized gradient approximation (GGA). However, the limitations of LDA and GGA in predicting band gaps pose serious problems to the description of the electronic and structural properties of oxygen vacancies in TiO_2.[20,21] The removal of an oxygen atom from the TiO_2 lattice results in a doubly occupied a_1 single-particle state in the band gap, that is very near the conduction-band minimum (CBM) in the LDA or GGA. When lattice relaxations are included, this a_1 state moves up in energy and merges with the conduction band. The two electrons are thus transferred to the CBM, rendering it impossible to stabilize a neutral or +1 charge state of the vacancy in which these electrons reside in localized states on the vacancy. Therefore, in the LDA or GGA, V_O behaves as a shallow donor. The question is whether this reflects the true physics of the V_O center or rather an artifact of LDA or GGA due to the underestimation of the band gap.

It is therefore necessary to use methods that overcome the band-gap problem in order to correctly describe the electronic and structural properties of the oxygen vacancy in TiO_2. Here we investigate the oxygen vacancy in rutile TiO_2 using the Heyd, Scuseria, and Ernzerhof (HSE) hybrid functional,[22] in which a portion of Hartree-Fock (HF) exchange is range limited and mixed with GGA exchange and correlation. HSE not only corrects the band gap of TiO_2 [see, e.g., Fig. 1(d)] but also stabilizes the neutral state in the band gap and thus provides the opportunity to correlate the position of the single-particle a_1 state with the local lattice relaxations. This allows us to compute formation energies and transition levels, and disentangle the effects of structural relaxations in the various charge states of V_O. The results show that the oxygen vacancy does act as a shallow donor.

II. COMPUTATIONAL APPROACH

The calculations are based on (generalized) Kohn-Sham theory[23] and the projector-augmented wave potentials[24,25] as implemented in the VASP code.[26,27] For Ti the 3*p*, 3*d*, and 4*s* states were treated as valence states and the Perdew, Burke, and Ernzerhof (PBE) potential with a core radius of 2.5 a.u was used whereas for O the standard PBE potential with a core radius of 1.5 a.u. was applied. The calculations were performed using both the GGA of PBE (Ref. 28) and the hybrid functional as proposed by HSE.[22] In the latter, the exchange potential is separated into a long-range and a short-range part, and HF exchange is mixed with PBE exchange only in the short-range part. The long-range part of the exchange potential is therefore essentially described by PBE.

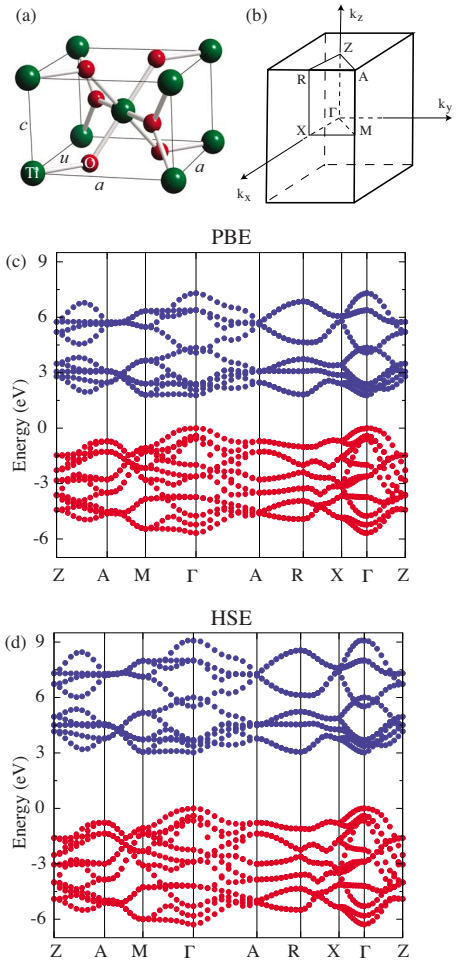

FIG. 1. (Color online) (a) Lattice parameters of TiO_2 in the rutile crystal structure. (b) Corresponding Brillouin zone. (c) and (d) calculated band structures using the GGA-PBE and HSE functionals. The valence-band maximum is set to zero in both cases.

In the present work, a consistent screening parameter of μ=0.2 $Å^{-1}$ is used for the semilocal (GGA) exchange as well as for the screened nonlocal exchange as suggested for the HSE06 functional.[29] Electronic correlation is represented by the corresponding part of the PBE functional. We find that a proportion of 20% HF exchange with 80% PBE exchange produces accurate values for lattice constants and the band gap in TiO_2.[30] From here on we will refer to this functional as "HSE."

Oxygen vacancies in rutile TiO_2 were simulated by removing one O atom from a supercell with 72 atoms. We used a plane-wave basis set with a cutoff of 400 eV and integrations over the Brillouin zone were perfomed using a $2\times2\times2$ mesh of special k points. The effects of the interactions between defects in neighboring supercells were minimized by performing additional calculations for supercells with 216 and 576 atoms, with two special k points [(0, 0, 0) and (1/2, 1/2. 1/2)]. The latter give the same results as a $2\times2\times2$ mesh for the supercell with 72 atoms. The results for different supercell sizes were used to extrapolate to the dilute limit, for which the defect-defect interactions are minimized. Calculations for odd charge states include the effects of spin polarization.

The relative stability of the various charge states is determined by the *formation energy*,

$$E^f(V_O^q) = E_t(V_O^q) - E_t(TiO_2) + \frac{1}{2}E_t(O_2) + \mu_O + qE_F, \quad (1)$$

where $E_t(V_O^q)$ is the total energy of the supercell containing a vacancy in charge state q and $E_t(TiO_2)$ is the total energy of a perfect crystal in the same supercell. The O atom that is removed from the crystal is placed in a reservoir of energy μ_O, referenced to the energy of oxygen in an isolated O_2 molecule. The chemical potential is a variable but must satisfy the stability condition of TiO_2, namely, $\mu_{Ti}+2\mu_O=\Delta H_f(TiO_2)$, where μ_{Ti} is the Ti chemical potential (referenced to bulk Ti). In the extreme O-rich limit, $\mu_O=0$. In the extreme Ti-rich limit, μ_{Ti} is bounded by the formation of Ti_2O_3, $2\mu_{Ti}+3\mu_O<\Delta H_f(Ti_2O_3)$, and, therefore, $\mu_{Ti}=2\Delta H_f(Ti_2O_3)-3\Delta H_f(TiO_2)$ and $\mu_O=-\Delta H_f(Ti_2O_3)+2\Delta H_f(TiO_2)$. The HSE calculated formation enthalpies $\Delta H_f(TiO_2)=-9.73$ eV and $\Delta H_f(Ti_2O_3)=-15.39$ eV are in good agreement with the experimental values.[31] The Fermi level E_F is the energy of the electron reservoir, referenced to the valence-band maximum (VBM). The latter includes a term obtained by aligning the electrostatic potential in a bulklike region of the defect supercell with the potential of the perfect crystal.[19] Madelung corrections for the electrostatic interaction between the homogeneous background charge and charged defects have not been included in the present work since the dielectric constants of TiO_2, in particular, the ionic contributions, are fairly large.

The value of the Fermi level where charge states q and q' are equal in energy defines the transition level $\varepsilon(q/q')$. Throughout this paper, when we use the terminology "+1" and "neutral" charge states we are referring to states in which electrons are bound to the defect center with *localized* wave functions. It may emerge that the resulting calculated transition levels are above the CBM; in such a case we may say that the +1 or neutral charge state is"unstable" since it is unlikely that the Fermi level would lie above the CBM in TiO_2 due to the extremely high density of electronic states near the CBM. It would, of course, be possible for one or two electrons to be bound, by Coulomb attraction, to the defect center; such states would be described by effective-mass theory, and would lead to a hydrogenic series of states just below the CBM. However, these hydrogenic states are not the focus of our current investigation. Our goal is to establish whether electrons can be bound to the vacancy in localized states, as opposed to extended effective-mass states.

III. RESULTS

A. Structural parameters and band structure of rutile TiO_2

TiO_2 in the rutile crystal structure can be described by a six-atom primitive cell with lattice parameters a and c, and an internal parameter u that defines the distance between Ti and O atoms in the plane perpendicular to the c direction, as shown in Fig. 1(a). The calculated lattice parameters using

TABLE I. Calculated structural parameters, band gap at Γ (E_g), and formation enthalpy (ΔH_f) of rutile TiO_2 using GGA-PBE and the HSE hybrid functional (using 20% HF exchange). The experimental values from Refs. 30–32 are also listed.

Functional	a (Å)	c/a	u/a	E_g	ΔH_f (eV)
PBE	4.65	0.639	0.305	1.77	−9.33
HSE	4.59	0.642	0.305	3.05	−9.73
Expt.	4.59	0.644		3.1	−9.74

both PBE and HSE are listed in Table I and are in very good agreement with the experimental values. The calculated band gaps are also listed in Table I, and the calculated band structures are shown in Figs. 1(c) and 1(d). Rutile TiO_2 has a direct band gap with the VBM and CBM both occurring at the Γ point. The indirect gaps Γ-M and Γ-R are less than 0.05 eV higher in energy. While the calculated band gap using PBE is only 1.77 eV, the HSE functional with 20% HF exchange produces a value of 3.05 eV, very close to the experimental value.[32]

B. HSE effects on the band structure of TiO_2

Before proceeding to the results for the oxygen vacancy in TiO_2, it is worthwhile to investigate how the HSE functional affects the positions of the VBM and CBM relative to PBE. Calculating this alignment requires going beyond mere bulk calculations; the latter only provide the positions of the VBM and CBM referenced to the average of the electrostatic potential, a quantity which is ill defined in calculations for perfect periodic crystals and therefore conventionally set to zero. An alignment of average electrostatic potentials can be obtained by performing surface calculations in a slab geometry, in which the potential inside the solid can be referenced to the potential in the vacuum region. Details of surface orientations and reconstructions in the slab calculation may, in principle, affect the absolute position of the VBM and CBM. However, by choosing a nonpolar surface and by focusing on *differences* between the values obtained by PBE and HSE using the same slab geometry (surface orientation and reconstruction), these effects largely cancel. In the present work, 11-layer slabs oriented along the [001] direction are employed. Convergence tests with respect to the slab thickness indicate that the error in the calculated band positions is less than 0.02 eV. Nonreconstructed ideal surfaces were used in order to avoid effects related to surface dipoles.

The effects of HSE on the band positions in TiO_2 are shown in Fig. 2. In HSE the VBM is lowered by 0.6 eV and the CBM is raised by 0.7 eV with respect to PBE. The lowering of the VBM in HSE can be attributed to the reduced self-interaction for the O 2*p*-derived states that compose the upper part of the valence band (Hartree-Fock is entirely self-interaction free). The upward shift of the CBM is also expected since Hartree-Fock generally increases band gaps. These effects of HSE on the VBM and CBM are taken into account in the following analysis of the oxygen vacancy.

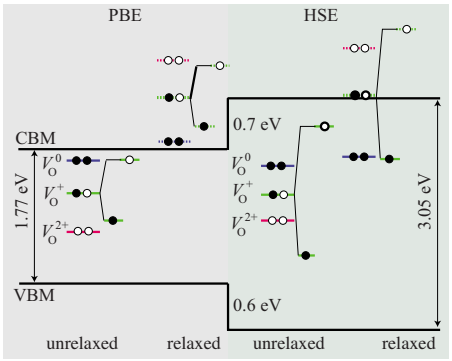

FIG. 2. (Color online) Calculated position of the single-particle a_1 state of the oxygen vacancy (V_O) in TiO_2. The PBE and HSE band structures were aligned as described in the text. The results for various charge states and for both unrelaxed and relaxed vacancies are shown. For V_O^+, the position of the a_1 state in both spin-up and spin-down channels is also indicated. The positions of states above the CBM were estimated based on projected densities of states on the three nearest-neighbor Ti atoms and are represented by dashed lines.

C. Oxygen vacancy: Electronic structure and lattice relaxations

The electronic and structural properties of the oxygen vacancy in TiO_2 can be qualitatively understood on the basis of molecular-orbital theory. Each oxygen atom in rutile TiO_2 is surrounded by three Ti atoms, two of them being equivalent by symmetry. The removal of an O atom from the TiO_2 lattice results in three Ti dangling bonds with mostly *d* character that point into the vacancy and are occupied by a total of two electrons. These three dangling bonds combine into a lower energy fully symmetric state (a_1 symmetry) and two higher-energy states; the point-group symmetry is reduced from D_{2d} for the perfect crystal to C_{2v}. The electron occupancy of the a_1 state determines the charge state of the oxygen vacancy. In the neutral charge state (V_O^0), the a_1 state is doubly occupied; in the +1 charge state (V_O^+), it is occupied by one electron; and in the +2 charge state (V_O^{2+}), it is empty.

The occupancy and the energetic position of the a_1 state are closely related to the local structural relaxations around V_O. Upon removal of an O atom the three nearest-neighbor Ti atoms tend to relax away from the vacancy in order to strengthen their bonding with the rest of the lattice. This outward relaxation decreases the overlap between the three Ti dangling bonds, shifting the a_1 state to higher energy. However, if the a_1 state is occupied, this upward shift incurs a cost in electronic energy. Therefore, the tendency of the Ti atoms to relax away from the vacancy is counterbalanced by the gain in electronic energy as the Ti atoms are kept closer to their nominal positions in the lattice. Based on this argument, it is instructive to analyze the position of the a_1 state before (unrelaxed) and after lattice relaxations. Consistent with this picture, in the HSE we obtain relatively small relaxations in the case of the neutral V_O^0 and V_O^+. For V_O^{2+}, in which the a_1 state is empty, a large outward relaxation is observed since there is no cost in electronic energy when the state is shifted up.

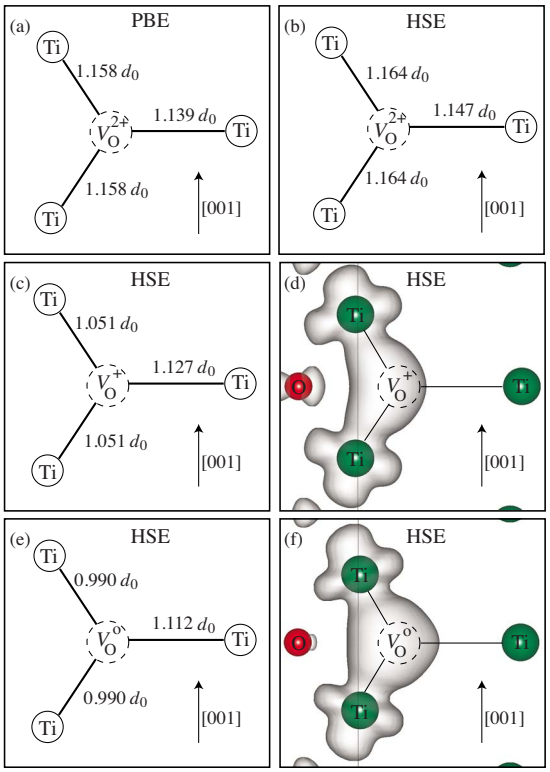

FIG. 3. (Color online) Panels (a) and (b) compare structural relaxations around V_O^{2+} in (a) GGA-PBE and (b) HSE. Panels (c)–(f) all show HSE results: (c) structural relaxations around V_O^{+}; (d) corresponding charge density of the a_1 state (spin-up channel); (e) structural relaxations around V_O^{0}; (f) corresponding charge density of the a_1 state. The isosurfaces in (d) and (f) correspond to 10% of the maximum of the charge density of the a_1 state in the supercell.

The position of the a_1 state relative to the VBM and CBM in PBE and HSE is shown in Fig. 2. In PBE, the doubly occupied a_1 state for the unrelaxed V_O^0 is slightly below the CBM. When structural relaxations are allowed, the Ti atoms move outward, the a_1 state merges with the conduction band, and the two electrons are transferred to the CBM. The defect then essentially consists of V_O^{2+} with two electrons in the conduction band. In PBE it is therefore impossible to stabilize V_O^0 and the same problem occurs for V_O^+. Therefore, only the V_O^{2+} charge state, in which the a_1 state is empty, is stable in PBE. However, due to the severe underestimation of the band gap, it is not clear whether the positive and neutral charge states might be stabilized if the band gap is corrected. This is what is addressed by our HSE calculations.

In HSE, the a_1 state of the unrelaxed V_O^0 is located at 0.9 eV below the CBM. Upon relaxation of the Ti atoms the a_1 is shifted up in energy by 0.2 eV, again indicating that the electronic energy gain by keeping the Ti atoms close to their nominal positions dominates in the neutral charge state. The resulting position of the a_1 state is still well below the CBM in HSE, i.e., the neutral charge state can indeed be stabilized (contrary to the PBE result). Removing one electron from the a_1 state causes the Ti atoms to move outward from the vacancy, and the occupied a_1 state (spin-up channel) is shifted up by 1.2 eV. The empty a_1 (spin-down channel) merges with the conduction band. This is also in contrast to the PBE result in which the a_1 (both spin-up and spin-down) merge with the conduction band after lattice relaxations are included. Removing the second electron from the a_1 state causes the Ti atoms to strongly relax outward and the a_1 state is raised even higher. Based on the HSE calculations we therefore conclude that V_O in rutile TiO_2 can, in principle, exist in three charge states, namely, neutral, +1, and +2.

The local lattice relaxations around V_O^0, V_O^+, and V_O^{2+} are shown in Fig. 3. The displacements of the Ti atoms around V_O^0 and V_O^+ are much smaller than those around V_O^{2+} for the reasons discussed above. The HSE calculations produce the interesting result that the lattice relaxations around V_O^0 and V_O^+ are asymmetric. The displacement of the Ti atom in the (001) plane through the vacancy is significantly larger than the displacements of the two equivalent out-of-plane Ti atoms. In the case of V_O^0, the out-of-plane Ti atoms relax slightly inward in order to increase the overlap of the d states that compose the a_1 state; in the case of V_O^+, the out-of-plane Ti atoms relax slightly outward. The charge densities corresponding to the a_1 state for V_O^0 and V_O^+ [Figs. 3(d) and 3(e)] are indeed more localized on and between the two out-of-plane Ti atoms, with almost no contribution from the in-plane Ti atom. The asymmetry in the relaxation is likely due to a reduction in the self-interaction error in HSE that gives rise to a stronger electron localization than in PBE. Similar asymmetric relaxations have previously been observed in Hartree-Fock (self-interaction free) calculations in the context of hole localization on the Mg vacancy or substitutional Li in magnesium oxide.[33,34]

D. Oxygen vacancy: Formation energies

The energetic position and correct occupation of the a_1 state relative to the CBM are essential for a proper description of the electronic structure of V_O in TiO_2. Ultimately, however, the relative stability of the various charge states is determined by the *formation energy*, as defined in Eq. (1). The calculated formation energies as a function of the Fermi level for the oxygen vacancy in TiO_2 using supercells of 72 atoms are shown in Fig. 4. For the *unrelaxed* vacancy [Figs. 2, 4(a), and 4(b)], the a_1 state resides in the band gap for all charge states in both PBE and HSE. As a consequence, the transition levels $\varepsilon(2+/+)$, $\varepsilon(+/0)$, and $\varepsilon(2+/0)$ are also located within the band gap. We note that the formation energies of V_O^0 are very similar in the PBE and HSE, consistent with the similar position of the doubly occupied a_1 state on an absolute energy scale [Fig. 2]. The observed difference in the formation energy of V_O^{2+} between PBE and HSE may be largely attributed to the difference in the position of the VBM shown in Fig. 2. Allowing structural relaxations lowers the formation energies of V_O^0 and V_O^+ by 0.3 and 0.9 eV, respectively, according to the HSE calculations; as discussed above, relaxed V_O^0 and V_O^+ are unstable in PBE. In the case of V_O^{2+} the structural relaxations lower the formation energy by comparable amounts in PBE (2.7 eV) and HSE (2.8 eV), consistent with the similar local lattice relaxations shown in Figs. 3(a) and 3(b).

In order to correct for the effects of using a finite-size supercell to simulate an isolated oxygen vacancy in TiO_2, we

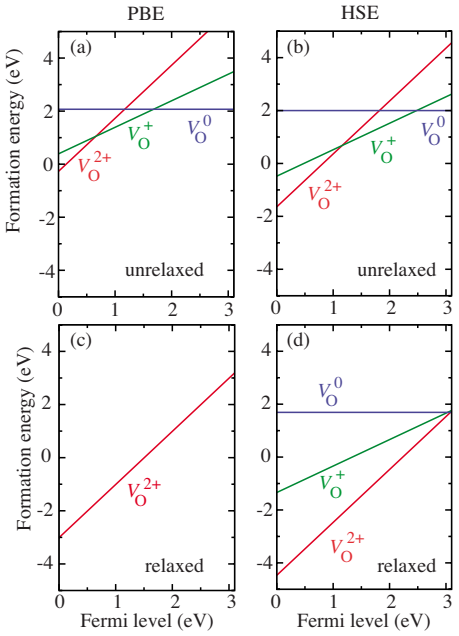

FIG. 4. (Color online) Comparison of PBE [(a) and (c)] and HSE [(b) and (d)] results for oxygen-vacancy formation energies in TiO_2 under Ti-rich (O-poor) conditions, for 72-atom supercells. (a) and (b) correspond to the unrelaxed case (without including structural relaxations); (c) and (d) correspond to the fully relaxed structures.

also performed calculations for supercells with 216 and 576 atoms using the PBE functional. Tests were performed using the HSE for the supercells with 216 atoms. We find that the formation energies of V_O^0 and V_O^+ change by less than 0.1 eV by extrapolating the results for 72-atom and 216-atom supercells to the dilute limit, consistent with the relatively small lattice relaxations reported above. However, for V_O^{2+} we find a somewhat larger correction of −0.7 eV by extrapolating the results of 72-atom, 216-atom, and 576-atom supercells to the dilute limit, consistent with the larger (and long-range) lattice relaxations around V_O^{2+} found in our calculations. We emphasize that the observed supercell-size dependence is due to the effect of long-range lattice relaxations, and not to interactions between periodic images of charged defects; the latter are efficiently screened due to the large dielectric constant of TiO_2.

The extrapolated formation energies for the oxygen vacancy in rutile TiO_2 for O-rich and Ti-rich limit conditions are shown in Fig. 5. According to HSE, the oxygen vacancy is a shallow donor in TiO_2. V_O^{2+} has the lowest formation energy for all values of the Fermi level in the band gap; the transition levels $\varepsilon(2+/+)$ and $\varepsilon(2+/0)$ are located above the CBM. Thus, we conclude that V_O^0 and V_O^+ are unstable, i.e., V_O with one or two electrons bound in localized states are always higher in energy than the doubly ionized V_O^{2+} center. Note that up to two electrons could be bound to the V_O^{2+} center in hydrogenic effective-mass states, making the center overall neutral. But we distinguish these hydrogenic states from the localized charge states that enter the definition of the formation energy in Eq. (1). The binding of an electron to a shallow donor is what happens in the case of any shallow donor in any semiconductor, and as such it is not discussed in the present work.

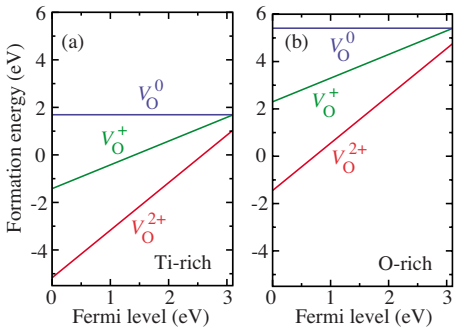

FIG. 5. (Color online) Calculated HSE formation energies for oxygen vacancies (V_O) in rutile TiO_2 as a function of Fermi level for (a) Ti-rich (O-poor) and (b) O-rich (Ti-poor) conditions. Corrections due to the finite size of the supercells are included as described in the text. States corresponding to one or two electrons bound to V_O^{2+} in extended effective-mass states, which would lie very close to the CBM, are not represented here.

According to HSE, the formation energy of V_O^{2+} is fairly low in *n*-type TiO_2 (Fermi level at the CBM) in the extreme Ti-rich (O-poor) limit. This formation energy would lead to an estimated equilibrium concentration of 3×10^{17} cm^{-3} at 1000 K. However, the formation energy increases with the oxygen chemical potential as shown in Fig. 5(b). This is consistent with experimental observations in which the electrical conductivity was found to decrease with oxygen partial pressure.[7–12]

E. Discussion

Several DFT calculations of oxygen vacancies in bulk TiO_2 have been reported.[20,21,35–38] References 20, 21, and 38 report calculations for V_O in anatase TiO_2 and Refs. 35–37 in the rutile phase. In both anatase and rutile the O atoms are threefold coordinated, and despite the differences in the bond angles and interatomic distances, we expect the electronic and structural properties of V_O to be similar in both phases. As such, we find that our PBE results for V_O^{2+} essentially agree with the results reported in Refs. 20, 21, and 35–37. Small differences arise due to the choice of the chemical potentials. In the present work and in Ref. 21, Ti_2O_3 is taken as the limiting phase in Ti-rich conditions but Refs. 20, 35, and 36 use bulk Ti as the limit. We emphasize that our results show that it is not possible to stabilize V_O^0 and V_O^+ in PBE when lattice relaxations are included. The results reported in Refs. 20, 35, and 36 seem to allow such a stabilization; however, we suggest that a detailed analysis of the band structures, Kohn-Sham state occupations, and lattice relaxations in those calculations would reveal that the alleged V_O^+ and V_O^0 actually consist of V_O^{2+} with one or two electrons in the conduction band, respectively.

We also note that the formation energy of V_O^{2+} in HSE is lower than in our PBE calculations or the LDA results reported in Refs. 20, 21, 35, and 36. This can be explained by the lowering of the absolute position of the valence band due

to the self-interaction corrections in HSE when we inspect the HSE results at $E_F=0.6$ eV (corresponding to the position of the VBM in PBE, as seen in Fig. 2), the formation energies are quite close to those obtained with PBE at $E_F=0$ (Fig. 4).

Finally, we compare our HSE results with the hybrid functional and GGA+U calculations for V_O^0 in anatase TiO_2 reported in Ref. 38. We find that our a_1 state is in the band gap and localized on two Ti atoms that are nearest neighbors to the vacancy. This is in contrast to the results of Ref. 38 which find the states also in the gap but localized on Ti atoms that are far away from the vacancy. We were able to stabilize similar solutions and found that these solutions have roughly the same energy as the solution shown in Fig. 3(f). However, such a state is better described as V_O^{2+} plus two electrons trapped at bulklike Ti sites, consistent with the results shown in Fig. 4(d). The issue of whether individual Ti sites in the bulk can trap electrons from the conduction band is unrelated to the intrinsic properties of the oxygen vacancy and hence beyond the scope of the present work. Unfortunately, the authors of Ref. 38 did not provide results for different charge states, and we cannot compare our calculated transition energies with their results.

IV. SUMMARY

In conclusion, the HSE hybrid functional calculations show V_O to be a shallow donor, stable in the V_O^{2+} configuration for all Fermi-level positions within the band gap, with the transition levels $\varepsilon(2+/+)$ and $\varepsilon(2+/0)$ located above the CBM. The formation energy of V_O^{2+} in n-type TiO_2 (Fermi level at the CBM) is about 1.0 eV under extreme oxygen-poor conditions. This formation energy of V_O^{2+} is low enough to, in principle, account for the observed n-type conductivity in TiO_2 single crystals annealed under Ti-rich (O-poor) conditions, and its dependence on oxygen chemical potential is also consistent with the observed variation in the electrical conductivity with oxygen partial pressure.

ACKNOWLEDGMENTS

This work was supported by the NSF MRSEC Program under Award No. DMR05-20415 and by the UCSB Solid State Lighting and Energy Center. It made use of the CNSI Computing Facility under NSF Grant No. CHE-0321368, and the Ranger supercomputer from the TeraGrid computing resources supported by the NSF under Grant No. DMR070072N. The work was also partly supported by the Austrian FWF within the START Grant No. Y218. P. Rinke acknowledges the Deutsche Forschungsgemeinschaft for financial support.

*Present address: Advanced Electronic Materials Center, National Institute for Materials Science, Tsukuba 305-0044, Japan.

[1] G. Wilk, R. Wallace, and J. Anthony, J. Appl. Phys. **89**, 5243 (2001).
[2] B. O'Regan and M. Grätzel, Nature (London) **353**, 737 (1991).
[3] A. Fujishima and K. Honda, Nature (London) **238**, 37 (1972).
[4] A. L. Linsebigler, G. Lu, and J. T. Yates, Jr., Chem. Rev. (Washington, D.C.) **95**, 735 (1995).
[5] N. Umezawa, A. Janotti, P. Rinke, T. Chikyow, and C. G. Van de Walle, Appl. Phys. Lett. **92**, 041104 (2008).
[6] E. Yagi, R. R. Hasiguti, and M. Aono, Phys. Rev. B **54**, 7945 (1996).
[7] J. Yahia, Phys. Rev. **130**, 1711 (1963).
[8] C. J. Kevane, Phys. Rev. **133**, A1431 (1964).
[9] L. Forro, O. Chauvet, D. Emin, L. Zuppiroli, H. Berger, and F. Levy, J. Appl. Phys. **75**, 633 (1994).
[10] J. Nowotny, M. Radecka, M. Rekas, S. Sugihara, E. R. Vance, and W. Weppner, Ceram. Int. **24**, 571 (1998).
[11] M. K. Nowotny, T. Bak, and J. Nowotny, J. Phys. Chem. B **110**, 16270 (2006).
[12] P. Kofstad, J. Less-Common Met. **13**, 635 (1967).
[13] U. Diebold, Surf. Sci. Rep. **48**, 53 (2003).
[14] M. Li, W. Hebenstreit, U. Diebold, A. M. Tyryshkin, M. K. Bowman, G. G. Dunham, and M. A. Henderson, J. Phys. Chem. B **104**, 4944 (2000).
[15] U. Diebold, M. Li, O. Dulub, E. L. D. Hebenstreit, and W. Hebenstreit, Surf. Rev. Lett. **7**, 613 (2000).
[16] L. S. Vlasenko and G. D. Watkins, Phys. Rev. B **72**, 035203 (2005).
[17] A. Janotti and C. G. Van de Walle, Appl. Phys. Lett. **87**, 122102 (2005).
[18] F. Oba, A. Togo, I. Tanaka, J. Paier, and G. Kresse, Phys. Rev. B **77**, 245202 (2008).
[19] C. G. Van de Walle and J. Neugebauer, J. Appl. Phys. **95**, 3851 (2004).
[20] J. M. Sullivan and S. C. Erwin, Phys. Rev. B **67**, 144415 (2003).
[21] S. Na-Phattalung, M. F. Smith, K. Kim, M.-H. Du, S.-H. Wei, S. B. Zhang, and S. Limpijumnong, Phys. Rev. B **73**, 125205 (2006).
[22] J. Heyd, G. E. Scuseria, and M. Ernzerhof, J. Chem. Phys. **118**, 8207 (2003); **124**, 219906(E) (2006).
[23] W. Kohn and L. J. Sham, Phys. Rev. **140**, A1133 (1965).
[24] P. E. Blöchl, Phys. Rev. B **50**, 17953 (1994).
[25] G. Kresse and D. Joubert, Phys. Rev. B **59**, 1758 (1999).
[26] G. Kresse and J. Furthmüller, Phys. Rev. B **54**, 11169 (1996).
[27] G. Kresse and J. Furthmüller, Comput. Mater. Sci. **6**, 15 (1996).
[28] J. P. Perdew, K. Burke, and M. Ernzerhof, Phys. Rev. Lett. **77**, 3865 (1996).
[29] A. V. Krukau, O. A. Vydrov, A. F. Izmaylov, and G. E. Scuseria, J. Chem. Phys. **125**, 224106 (2006).
[30] F. A. Grant, Rev. Mod. Phys. **31**, 646 (1959).
[31] G. V. Samsonov, *The Oxide Handbook* (IFI/Plenum, New York, 1982).
[32] A. Amtout and R. Leonelli, Phys. Rev. B **51**, 6842 (1995).
[33] P. Baranek, G. Pinarello, C. Pisani, and R. Dovesi, Phys. Chem. Chem. Phys. **2**, 3893 (2000).
[34] A. Lichanot, C. Larrieu, R. Orlando, and R. Dovesi, J. Phys. Chem. Solids **59**, 7 (1998).

[35] E. Cho, S. Han, H. S. Ahn, K. R. Lee, S. K. Kim, and C. S. Hwang, Phys. Rev. B **73**, 193202 (2006).
[36] H. Iddir, S. Ogut, P. Zapol, and N. D. Browning, Phys. Rev. B **75**, 073203 (2007).
[37] J. He, R. K. Behera, M. W. Finnis, X. Li, E. C. Dickey, S. R. Phillpot, and S. B. Sinnott, Acta Mater. **55**, 4325 (2007).
[38] E. Finazzi, C. Valentin, G. Pacchioni, and A. Selloni, J. Chem. Phys. **129**, 154113 (2008).